# Recent Applications of Nuclear Quantum Monte Carlo

Robert B. Wiringa, Physics Division, Argonne National Laboratory

Joseph Carlson, Los Alamos

Gerald A. Miller, Seattle

Saori Pastore, South Carolina

Steven C. Pieper, Argonne

Rocco Schiavilla, JLab & ODU

WORK NOT POSSIBLE WITHOUT EXTENSIVE COMPUTER RESOURCES

Argonne Laboratory Computing Resource Center (Fusion & Blues)

Argonne Leadership Computing Facility (BlueGene/P & /Q)


Physics Division

Work supported by U.S. Department of Energy, Office of Nuclear Physics

B. Day

IL NUOVO CIMENTO Vol. 25 A, N. 4 21 Febbraio 1975

# The Hypernetted-Chain Approximation for a Fermion System.

S. FANTONI and S. ROSATI

*Istituto di Fisica dell'Università - Pisa*

(ricevuto il 2 Agosto 1974)

**Summary.** — An iterative procedure is presented to exactly calculate the two-body distribution function of an infinite fermion system described by a Jastrow wave function of general product form. In the approximation of neglecting the elementary diagrams the procedure leads to integral equations which are the analogues of the well-known hypernetted-chain equation for the boson case. Preliminary numerical calculations have been performed for the ground state of nuclear matter using central, hard-core $N$-$N$ potentials; the results obtained seem to indicate the necessity of using the fermion HNC approximation even at nuclear densities.


Workshop on Nuclear and Dense Matter, May 3-6, 1977, Urbana, Illinois

# *Ab Initio* Calculations of Light Nuclei

## Goals

Understand nuclei at the level of elementary interactions between individual nucleons, including

- Binding energies, excitation spectra, relative stability
- Densities, electromagnetic moments, transition amplitudes, cluster-cluster overlaps
- Low-energy $NA$ & $AA'$ scattering, asymptotic normalizations, astrophysical reactions

## Requirements

- Two-nucleon potentials that accurately describe elastic $NN$ scattering data
- Consistent three-nucleon potentials and two-nucleon electroweak current operators
- Accurate methods for solving the many-nucleon Schrödinger equation

## Results

- Quantum Monte Carlo methods can evaluate realistic Hamiltonians accurate to $\sim$1–2%
- About 100 states calculated for $A \leq 12$ nuclei in good agreement with experiment
- Applications to elastic & ineleastic $e, \pi$ scattering, $(e, e'p)$, $(d, p)$ reactions, etc.
- Electromagnetic moments, $M1$, $E2$, F, GT transitions calculated
- $^5$He = $n\alpha$ scattering and $3 \leq A \leq 9$ ANCs and widths

# NUCLEAR HAMILTONIAN

$$H = \sum_i K_i + \sum_{i<j} v_{ij} + \sum_{i<j<k} V_{ijk}$$

$$K_i = -\frac{\hbar^2}{4}\left[\left(\frac{1}{m_p} + \frac{1}{m_n}\right) + \left(\frac{1}{m_p} - \frac{1}{m_n}\right)\tau_{iz}\right]\nabla_i^2$$

Wiringa, Stoks, & Schiavilla, PRC **51**, 38 (1995)

## Argonne $v_{18}$

$v_{ij} = v_{ij}^{\gamma} + v_{ij}^{\pi} + v_{ij}^{I} + v_{ij}^{S} = \sum v_p(r_{ij}) O_{ij}^p$

$v_{ij}^{\gamma}$: $pp$, $pn$ & $nn$ electromagnetic terms

$v_{ij}^{\pi} \sim [Y_\pi(r_{ij})\sigma_i \cdot \sigma_j + T_\pi(r_{ij}) S_{ij}] \otimes \tau_i \cdot \tau_j$

$v_{ij}^{I} = \sum_p I^p T_\pi^2(r_{ij}) O_{ij}^p$

$v_{ij}^{S} = \sum_p [P^p + Q^p r + R^p r^2] W(r) O_{ij}^p$


$$\begin{aligned} O_{ij}^p = & [1, \sigma_i \cdot \sigma_j, S_{ij}, \mathbf{L}\cdot\mathbf{S}, \mathbf{L}^2, \mathbf{L}^2(\sigma_i \cdot \sigma_j), (\mathbf{L}\cdot\mathbf{S})^2] \\ & + [1, \sigma_i \cdot \sigma_j, S_{ij}, \mathbf{L}\cdot\mathbf{S}, \mathbf{L}^2, \mathbf{L}^2(\sigma_i \cdot \sigma_j), (\mathbf{L}\cdot\mathbf{S})^2] \otimes \tau_i \cdot \tau_j \\ & + [1, \sigma_i \cdot \sigma_j, S_{ij}, \mathbf{L}\cdot\mathbf{S}] \otimes T_{ij} \\ & + [1, \sigma_i \cdot \sigma_j, S_{ij}, \mathbf{L}\cdot\mathbf{S}] \otimes (\tau_i + \tau_j)_z \end{aligned}$$

Argonne $v_{18}$ fitted to Nijmegen PWA93 data base of 1787 $pp$ & 2514 $np$ observables for $E_{lab} \leq 350$ MeV with $\chi^2$/datum = 1.1 plus $nn$ scattering length & $^2$H binding energy

# THREE-NUCLEON POTENTIALS

Urbana $V_{ijk} = V_{ijk}^{2\pi P} + V_{ijk}^{R}$

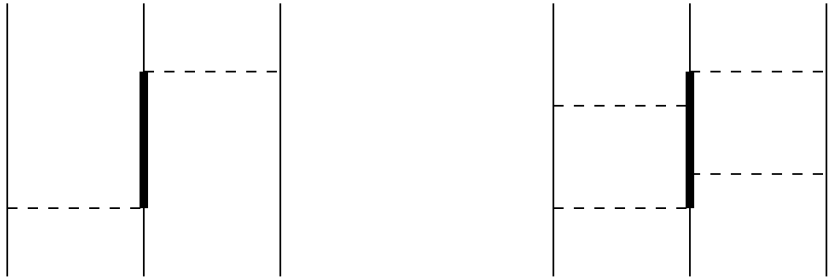

Carlson, Pandharipande, & Wiringa, NP **A401**, 59 (1983)

Illinois $V_{ijk} = V_{ijk}^{2\pi P} + V_{ijk}^{2\pi S} + V_{ijk}^{3\pi\Delta R} + V_{ijk}^{R}$

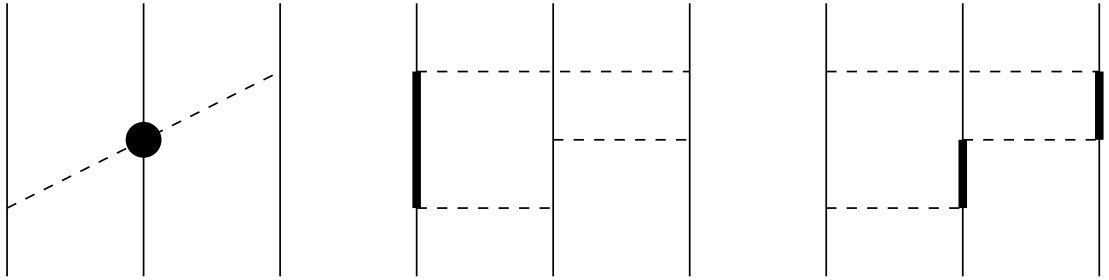

Pieper, Pandharipande, Wiringa, & Carlson, PRC **64**, 014001 (2001)

Illinois-7 has 4 strength parameters fit to 23 energy levels in $A \leq 10$ nuclei.

In light nuclei we find (thanks to large cancellation between $\langle K \rangle$ & $\langle v_{ij} \rangle$):

$$\langle V_{ijk} \rangle \sim (0.02 \text{ to } 0.07)\, \langle v_{ij} \rangle \sim (0.15 \text{ to } 0.5)\, \langle H \rangle$$

We expect $\langle \mathcal{V}_{ijkl} \rangle \sim 0.05\, \langle V_{ijk} \rangle \sim (0.01 \text{ to } 0.03)\, \langle H \rangle \sim 1$ MeV in $^{12}$C .

# Variational Monte Carlo

Minimize expectation value of $H$

$$E_V = \frac{\langle \Psi_V | H | \Psi_V \rangle}{\langle \Psi_V | \Psi_V \rangle} \geq E_0$$

using Metropolis Monte Carlo and trial function

$$|\Psi_V\rangle = \left[ \mathcal{S} \prod_{i<j} (1 + U_{ij} + \sum_{k \neq i,j} U_{ijk}) \right] \left[ \prod_{i<j} f_c(r_{ij}) \right] |\Phi_A(JMTT_3)\rangle$$

- single-particle $\Phi_A(JMTT_3)$ is fully antisymmetric and translationally invariant
- central pair correlations $f_c(r)$ keep nucleons at favorable pair separation
- pair correlation operators $U_{ij} = \sum_p u_p(r_{ij}) O_{ij}^p$ reflect influence of $v_{ij}$
- triple correlation operator $U_{ijk}$ added when $V_{ijk}$ is present
- multiple $J^\pi$ states constructed and diagonalized for p-shell nuclei
- ability to construct clusterized or asymptotically correct trial functions

$\Psi_V$ are spin-isospin vectors in $3A$ dimensions with $\sim 2^A \binom{A}{Z}$ components

Lomnitz-Adler, Pandharipande, & Smith, NP **A361**, 399 (1981)
Wiringa, PRC **43**, 1585 (1991)

# GREEN'S FUNCTION MONTE CARLO

Projects out lowest energy state from variational trial function

$$\Psi(\tau) = \exp[-(H - E_0)\tau]\Psi_V = \sum_n \exp[-(E_n - E_0)\tau]a_n\psi_n$$

$$\Psi(\tau \to \infty) = a_0\psi_0$$

Evaluation of $\Psi(\tau)$ done stochastically in small time diffusion steps $\Delta\tau$

$$\Psi(\mathbf{R}_n, \tau) = \int G(\mathbf{R}_n, \mathbf{R}_{n-1}) \cdots G(\mathbf{R}_1, \mathbf{R}_0)\Psi_V(\mathbf{R}_0)d\mathbf{R}_{n-1} \cdots d\mathbf{R}_0$$

Mixed estimates used for expectation values

$$\langle O(\tau)\rangle = \frac{\langle\Psi(\tau)|O|\Psi(\tau)\rangle}{\langle\Psi(\tau)|\Psi(\tau)\rangle} \approx \langle O(\tau)\rangle_{\rm Mixed} + [\langle O(\tau)\rangle_{\rm Mixed} - \langle O\rangle_V]$$

$$\langle O(\tau)\rangle_{\rm Mixed} = \frac{\langle\Psi_V|O|\Psi(\tau)\rangle}{\langle\Psi_V|\Psi(\tau)\rangle} \quad ; \quad \langle H(\tau)\rangle_{\rm Mixed} = \frac{\langle\Psi(\tau/2)|H|\Psi(\tau/2)\rangle}{\langle\Psi(\tau/2)|\Psi(\tau/2)\rangle} \geq E_0$$

- Cannot propagate $p^2$, $L^2$, or $(\mathbf{L}\cdot\mathbf{S})^2$ operators $\Rightarrow$ use $H'$ = AV8′ + $\tilde{V}_{ijk}$
- Fermion sign problem would limit maximum $\tau$, but ...
- Constrained-path propagation removes steps that have $\Psi^\dagger(\tau, \mathbf{R})\Psi_V(\mathbf{R}) = 0$
- Multiple excited states of same $J^\pi$ stay orthogonal


Pudliner, Pandharipande, Carlson, Pieper, & Wiringa, PRC **56**, 1720 (1997)
Wiringa, Pieper, Carlson, & Pandharipande, PRC **62**, 014001 (2000)
Pieper, Wiringa, & Carlson, PRC **70**, 054325 (2004)

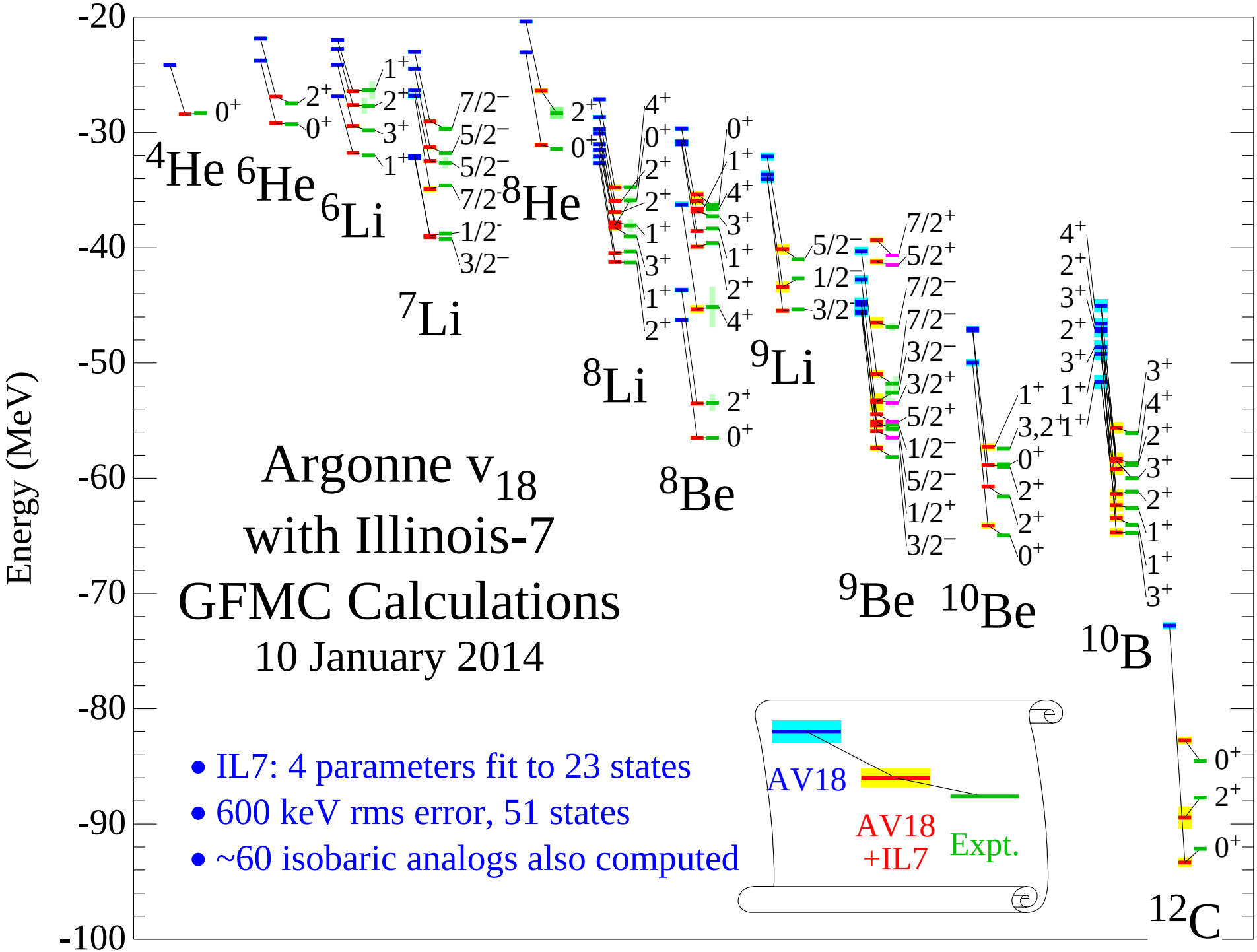
Energy (MeV)
-20
-30
-40
-50
-60
-70
-80
-90
-100
4He
6He
6Li
7Li
8He
8Li
8Be
9Li
9Be
10Be
10B
12C
Argonne v18
with Illinois-7
GFMC Calculations
10 January 2014
• IL7: 4 parameters fit to 23 states
• 600 keV rms error, 51 states
• ~60 isobaric analogs also computed
AV18
AV18
+IL7
Expt.

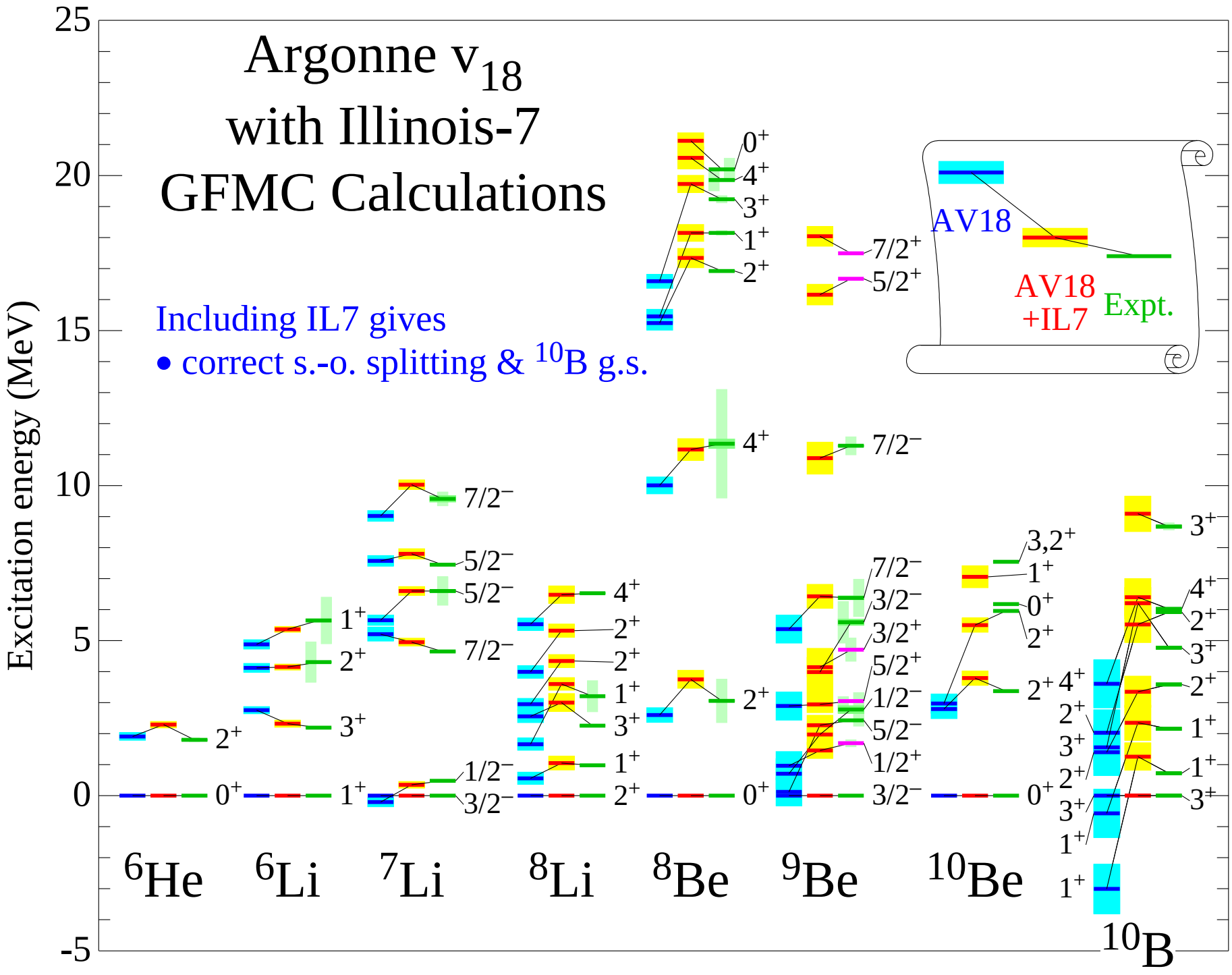
Argonne v18
with Illinois-7
GFMC Calculations
Including IL7 gives
• correct s.-o. splitting & 10B g.s.
AV18
AV18
+IL7
Expt.
Excitation energy (MeV)
25
20
15
10
5
0
-5
6He
6Li
7Li
8Li
8Be
9Be
10Be
10B

# Nolen-Schiffer Anomaly

Nuclear forces are mostly charge-independent [CI $\propto 1, \tau_i \cdot \tau_j$ ], but have small charge-dependent [CD $\propto T_{ij}$] and charge-symmetry-breaking [CSB $\propto (\tau_i + \tau_j)_z$] components, while electromagnetic forces are a mix of CI, CD, & CSB terms. Evidence for strong charge-independence-breaking (CIB) comes from the energy differences of isobaric multiplets:

$$E_{A,T}(T_z) = \sum_{n \leq 2T} a_n(A,T) Q_n(T,T_z)$$

$$Q_0 = 1 \; ; \; Q_1 = T_z \; ; \; Q_2 = \tfrac{1}{2}(3T_z^2 - T^2)$$

For example,

$$a_1(3, \tfrac{1}{2}) = E(^3\mathrm{He}) - E(^3\mathrm{H}) \qquad a_2(6,1) = \tfrac{1}{3}[E(^6\mathrm{Be}) - 2E(^6\mathrm{Li}^*) + E(^6\mathrm{He})]$$

The Nolen-Schiffer anomaly is the difference not explained by Coulomb force; strong CIB and other electromagnetic terms in Argonne $v_{18}$ explain much of the remainder (shown in keV):

| $a_n(A,T)$ | $K^{CSB}$ | $v_{C1}(pp)$ | $v^{\gamma,R}$ | $v^{CSB}$ +$v^{CD}$ | $\delta H^{CI}$ | Total | Expt. |
|---|---|---|---|---|---|---|---|
| $a_1(3, \frac{1}{2})$ | 14 | 642(1) | 26 | 65(0) | 8(1) | 755(1) | 764 |
| $a_1(7, \frac{1}{2})$ | 23 | 1442(2) | 36 | 83(1) | 27(10) | 1611(10) | 1645 |
| $a_1(8,1)$ | 25 | 1652(3) | 18 | 77(1) | 33(11) | 1813(11) | 1770 |
| $a_2(6,1)$ | | 140(1) | 18 | 100(2) | 17(2) | 273(3) | 223 |
| $a_2(8,1)$ | | 133(1) | 3 | −3(2) | 10(5) | 139(5) | 127 |

Wiringa, Pastore, Pieper, & Miller, Phys. Rev. C **88**, 044333 (2013)

# Isospin-mixing in $^8$Be

Experimental energies of $2^+$ states

$E_a$ = 16.626(3) MeV $\Gamma_a^\alpha$ = 108.1(5) keV

$E_b$ = 16.922(3) MeV $\Gamma_b^\alpha$ = 74.0(4) keV

Isospin mixing of $2^+;1$ and $2_2^+;0$ states due to isovector interaction $H_{01}$:

$\Psi_a = \beta\Psi_0 + \gamma\Psi_1$ ; $\Psi_b = \gamma\Psi_0 - \beta\Psi_1$

decay through $T = 0$ component only

$\Gamma_a^\alpha/\Gamma_b^\alpha = \beta^2/\gamma^2 \Rightarrow \beta = 0.77$ ; $\gamma = 0.64$

$$E_{a,b} = \frac{H_{00}+H_{11}}{2} \pm \sqrt{\left(\frac{H_{00}-H_{11}}{2}\right)^2 + (H_{01})^2}$$

$H_{00} = 16.746(2)$ MeV

$H_{11} = 16.802(2)$ MeV

$H_{01} = -145(3)$ keV

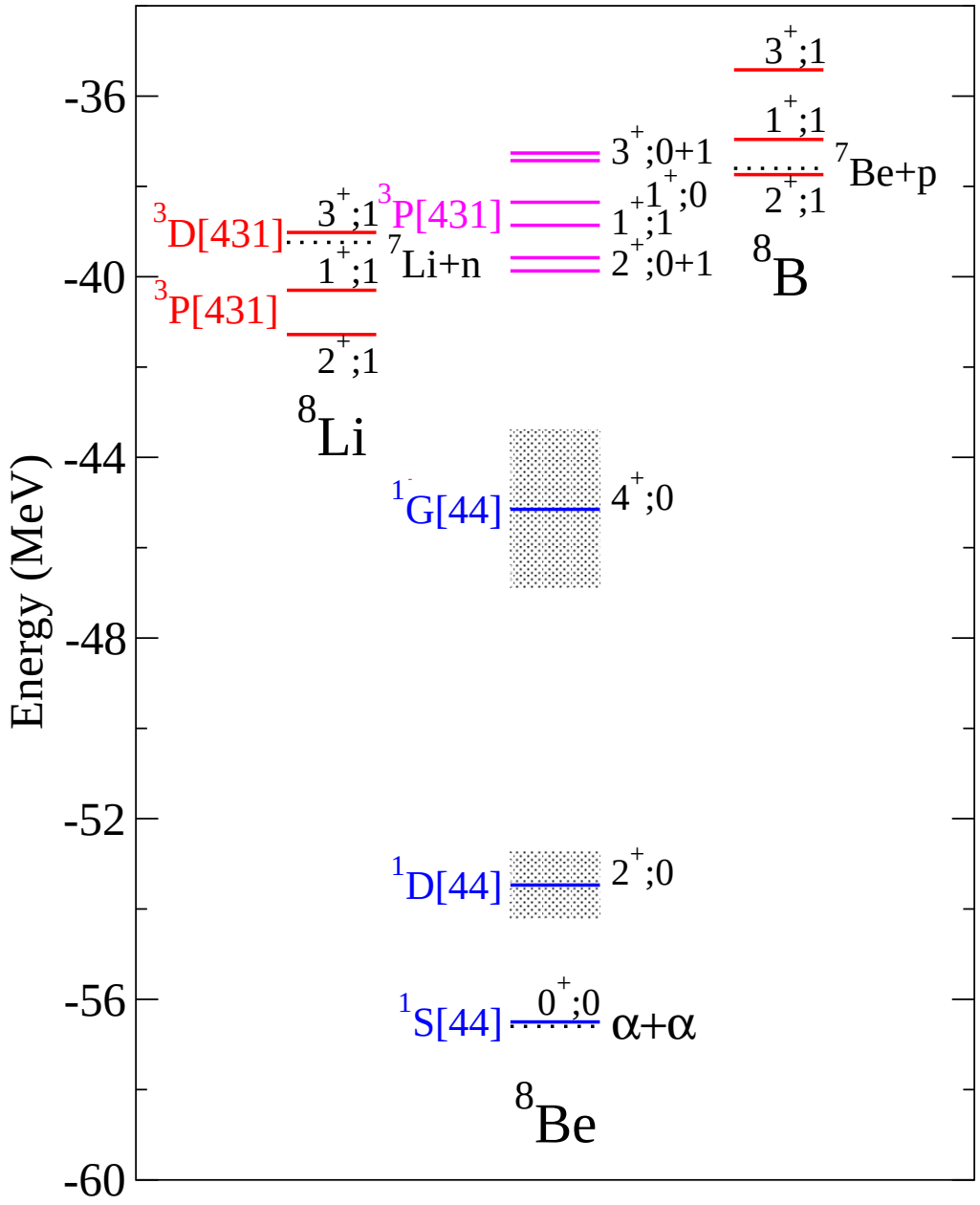

Isospin-mixing matrix elements in keV

| | $K^{CSB}$ | $v_{C1}(pp)$ | $v^{\gamma,R}$ | $v^{CSB}$ | $H_{01}$ | Expt. |
|---|---|---|---|---|---|---|
| $2^+;1 \Leftrightarrow 2^+_2;0$ | $-3.6(1)$ | $-89.3(11)$ | $-11.0(2)$ | $-23.4(4)$ | $-127(2)$ | $-145(3)$ |
| $1^+;1 \Leftrightarrow 1^+;0$ | $-2.8(1)$ | $-73.4(11)$ | $1.0(1)$ | $-18.5(4)$ | $-94(1)$ | $-103(14)$ |
| $3^+;1 \Leftrightarrow 3^+;0$ | $-3.0(1)$ | $-74.6(12)$ | $-16.8(2)$ | $-16.6(4)$ | $-111(2)$ | $-59(12)$ |
| $2^+;1 \Leftrightarrow 2^+_1;0$ | | | | | $-7(2)$ | |
| $0^+;2 \Leftrightarrow 0^+_3;0$ | | $-32.2(2)$ | $-8.9(1)$ | $-83.8(22)$ | $-125(2)$ | |

Coulomb terms are 70% of $H_{01}$, but magnetic moment and strong Type III CSB are relatively more important than in Nolen-Schiffer anomaly; still missing $\approx 10\%$ of strength.

Strong Type IV CSB also contribute (probably best nuclear structure place to look):

$$\begin{aligned} V_{IV}^{CSB} &= (\tau_1 - \tau_2)_z (\sigma_1 - \sigma_2) \cdot \mathbf{L}\, v(r) \\ &+ (\tau_1 \times \tau_2)_z (\sigma_1 \times \sigma_2) \cdot \mathbf{L}\, w(r) \end{aligned}$$

These contributions are model-dependent with $V_{IV}^{CSB} \sim \pm$ few keV.

Wiringa, Pastore, Pieper & Miller, Phys. Rev. C **88**, 044333 (2013)

# Single-Nucleon Momentum Distributions

Momentum distributions of nucleons and nucleon clusters can provide useful insights into various reactions on nuclei, such as $(e, e'p)$ and $(e, e'pN)$ electrodisintegration processes.

Probability of finding a nucleon in a nucleus with momentum $\mathbf{k}$ in a given spin-isospin state:

$$\rho_{\sigma\tau}(\mathbf{k}) = \int d\mathbf{r}'_1 d\mathbf{r}_1 d\mathbf{r}_2 \cdots d\mathbf{r}_A \, \psi^\dagger_{JM_J}(\mathbf{r}'_1, \mathbf{r}_2, \ldots, \mathbf{r}_A) \, e^{-i\mathbf{k}\cdot(\mathbf{r}_1 - \mathbf{r}'_1)} \, P_{\sigma\tau}(1) \, \psi_{JM_J}(\mathbf{r}_1, \mathbf{r}_2, \ldots, \mathbf{r}_A)$$

where $P_{\sigma\tau}$ is a spin-isospin projection operator and the normalization is:

$$N_{\sigma\tau} = \int \frac{d\mathbf{k}}{(2\pi)^3} \, \rho_{\sigma\tau}(\mathbf{k})$$

$N_{\sigma\tau}$ is the total number of nucleons with given spin-isospin.

Compute the Fourier transform by Metropolis Monte Carlo integration, using a standard Metropolis walk, guided by $|\Psi_{JM_J}(\mathbf{r}_1, \ldots, \mathbf{r}_i, \ldots, \mathbf{r}_A)|^2$ to sample configurations.
Average over all particles $i$ in each configuration; for each particle use a grid of Gauss-Legendre points $\mathbf{x}_i$ in a randomly chosen direction and move positions in both left- and right-hand side wave functions symmetrically away from their central value:

$$\rho_{\sigma\tau}(\mathbf{k}) = \frac{1}{A} \sum_i \int d\mathbf{r}_1 \cdots d\mathbf{r}_i \cdots d\mathbf{r}_A \int d\mathbf{\Omega}_x \int_0^{x_{\max}} x^2 dx \, \psi^\dagger_{JM_J}(\mathbf{r}_1, \ldots, \mathbf{r}_i + \mathbf{x}/2, \ldots, \mathbf{r}_A)$$

$$e^{-i\mathbf{k}\cdot\mathbf{x}} \, P_{\sigma\tau}(i) \, \psi_{JM_J}(\mathbf{r}_1, \ldots, \mathbf{r}_i - \mathbf{x}/2, \ldots, \mathbf{r}_A)$$

Deuteron proton momentum distribution has contributions from the $S$- and $D$-wave components of the wave function; $S$-wave has node at 2 fm$^{-1}$ that $D$-wave fills in to give a broad high-momentum shoulder out to $> 7$ fm$^{-1}$ before the second $S$-wave and first $D$-wave node.

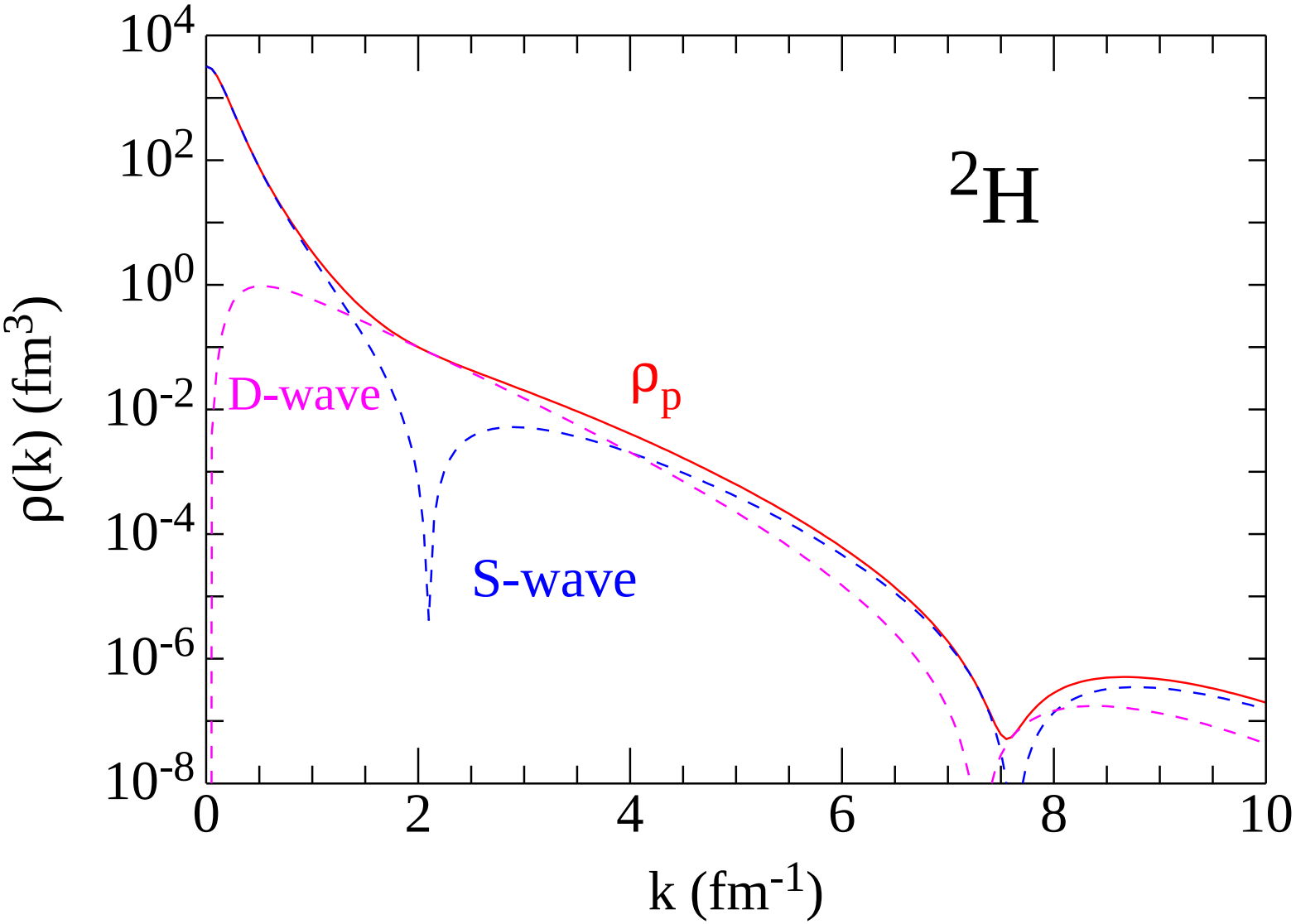

$^3$He in the $M_J = \frac{1}{2}^+$ state has spin-up proton and neutron distributions very similar to the deuteron, while the spin-down proton distribution is slightly larger, particularly in the dip region; the spin-down neutron distribution has a typical $D$-wave shape and is present due to the 9% $D$-state in the trinucleon wave function.

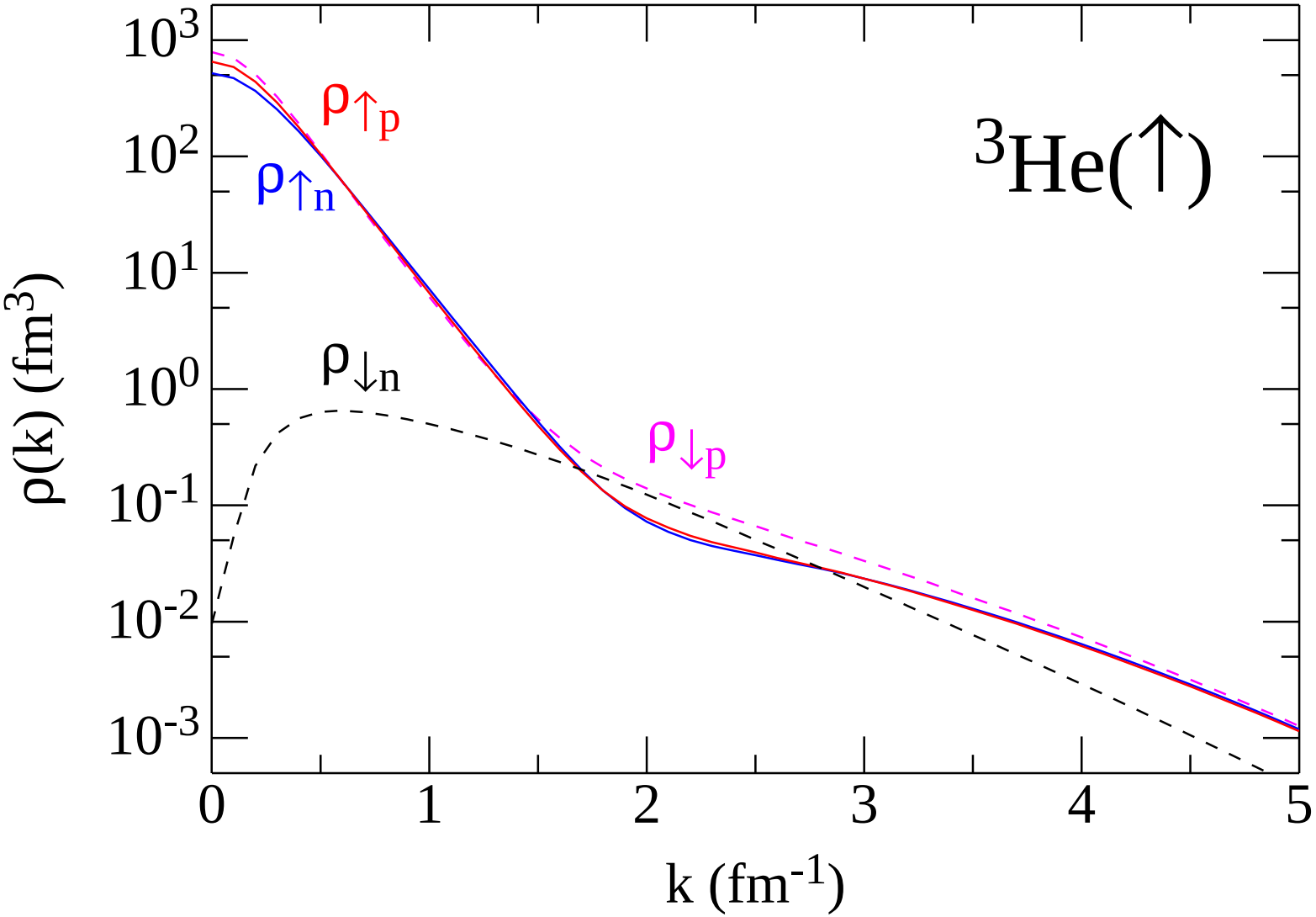

$^4$He proton momentum distribution is similar to deuteron, but less peaked at $k = 0$ because of greater binding, and a higher shoulder because of 15% $D$-state. AV18 alone has less binding and 13% $D$-state, so $3N$ force shifts the proton distribution to higher momenta. AV18(J) is from pure central Jastrow wave function and AV18(4) is with spin-isospin, but no tensor, correlations.

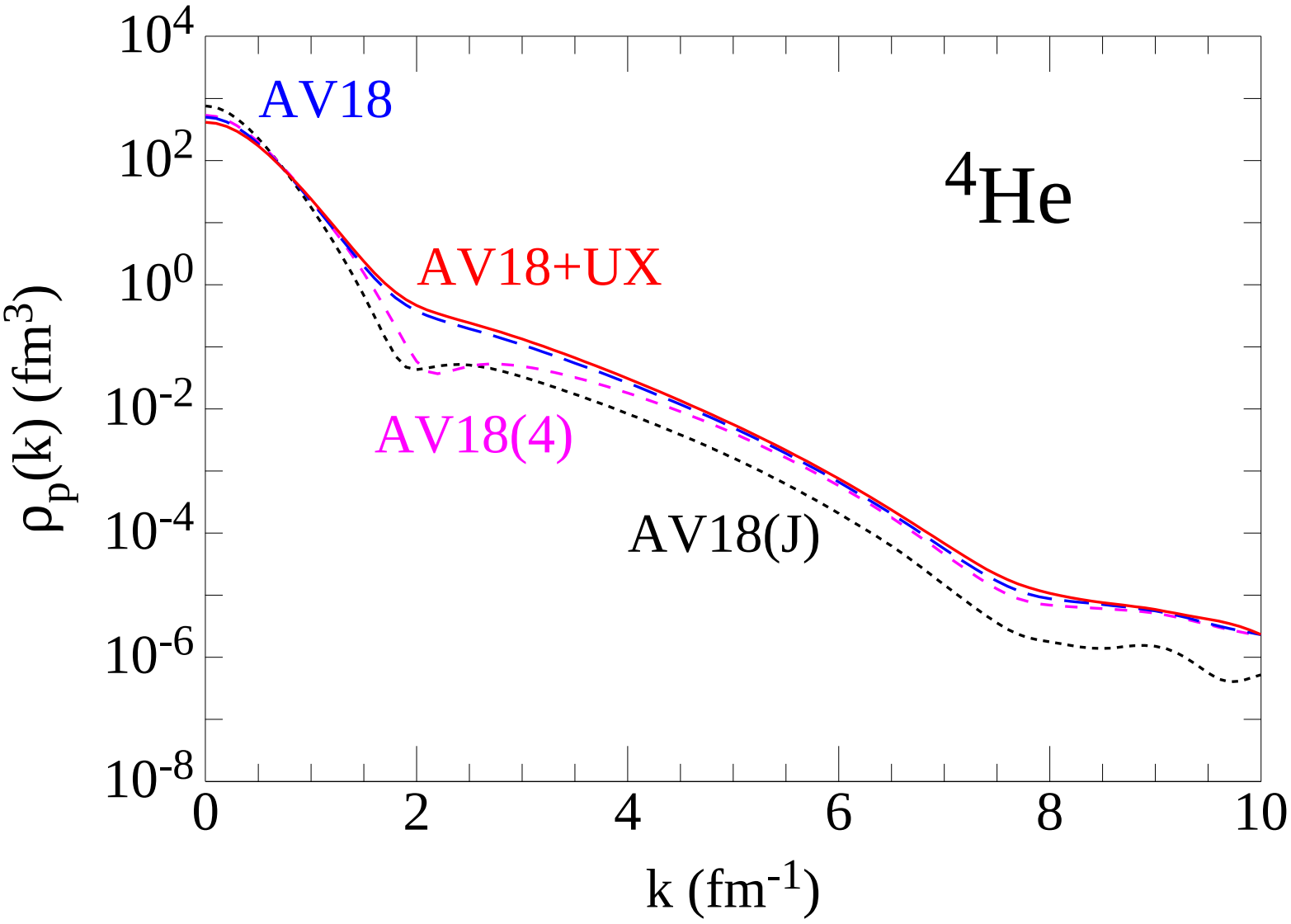

$^6$He proton momentum distribution is very similar to $^4$He, while neutron distribution peaks at $k > 0$ because of added $p$-shell neutrons; $(\rho_n - \rho_p)$ difference approximates the halo neutron distribution, where the two neutrons are primarily in a relative $S$-wave with corresponding dip.

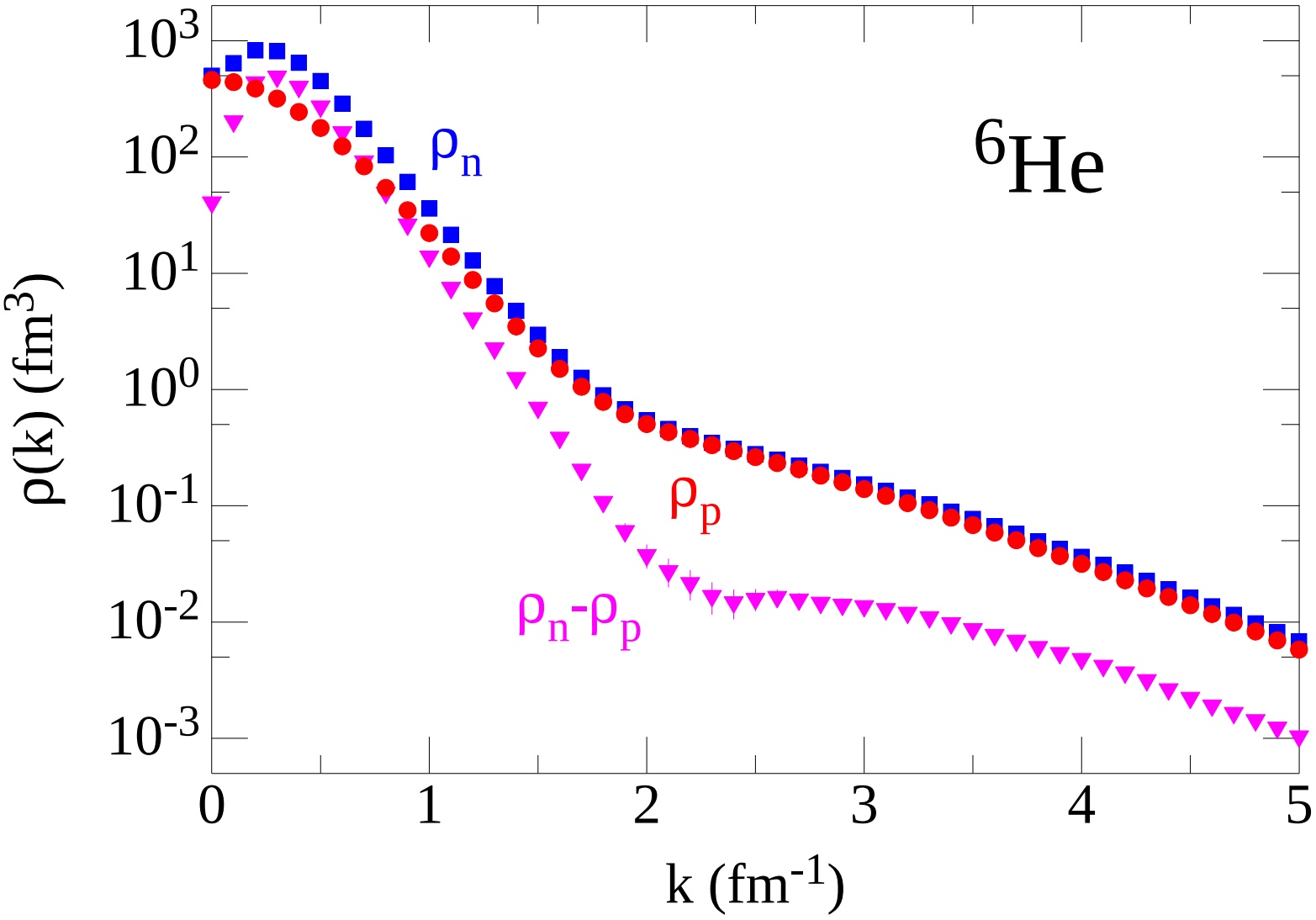

$^{8}$Be proton momentum distribution is again very similar to $^{4}$He. Also shown are the $\alpha$-$\alpha$ cluster distributions for the $0^+$ ground state, and the $2^+$ rotational state at 3 MeV excitation. At very low momenta, the nucleus is primarily in an $\alpha$-$\alpha$ cluster; the two nodes in $\rho_{\alpha\alpha}(0^+)$ indicate a relative 2*s* state, while the $\rho_{\alpha\alpha}(2^+)$ has a relative 1*d* state.

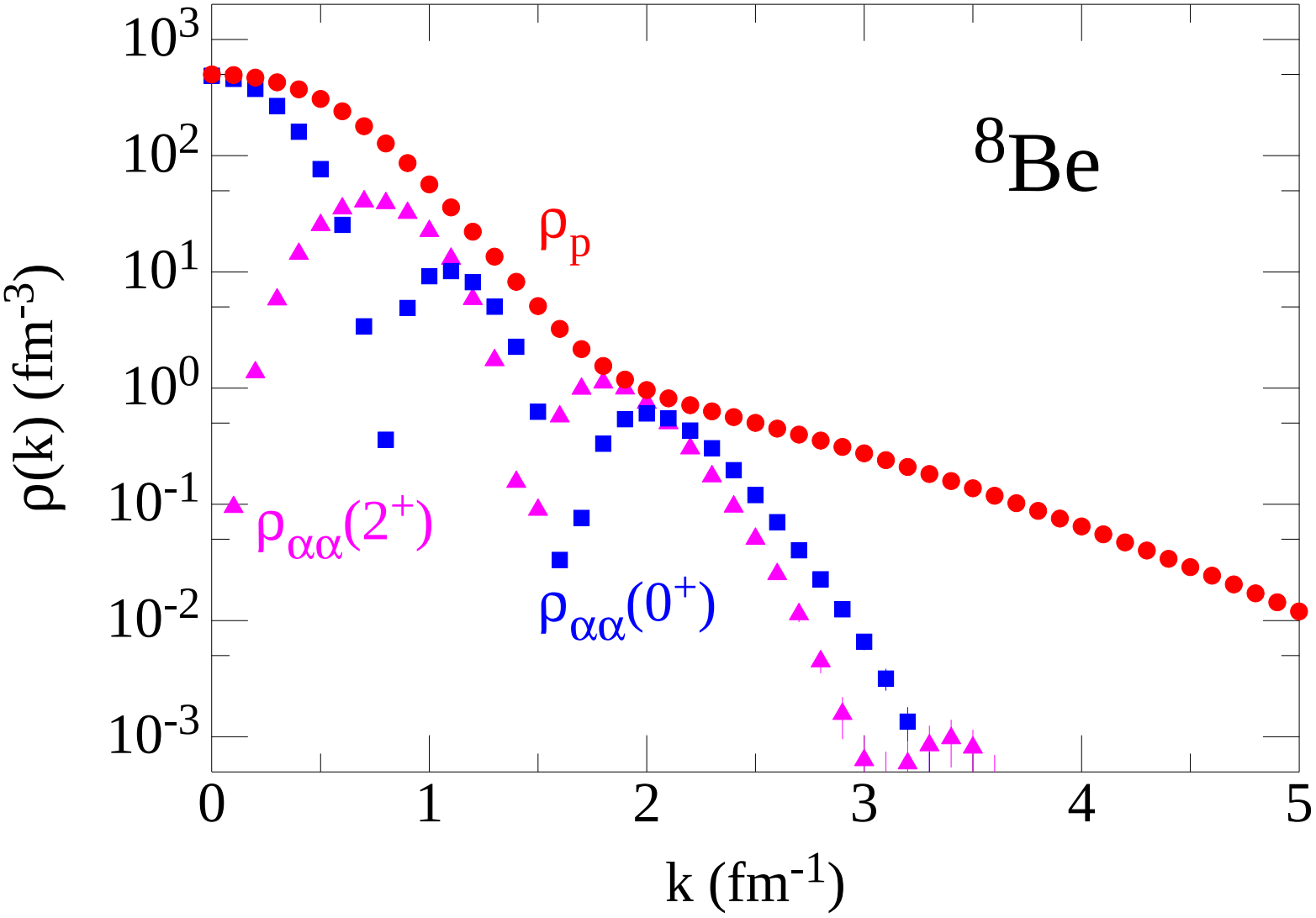

The proton momentum distributions in $T = 0$ light nuclei all have similar shapes, with the $k = 0$ peak decreasing in magnitude and broadening out as the binding increases and $p$-shell nucleons are added. The high momentum shoulder due to pion-exchange is universal.

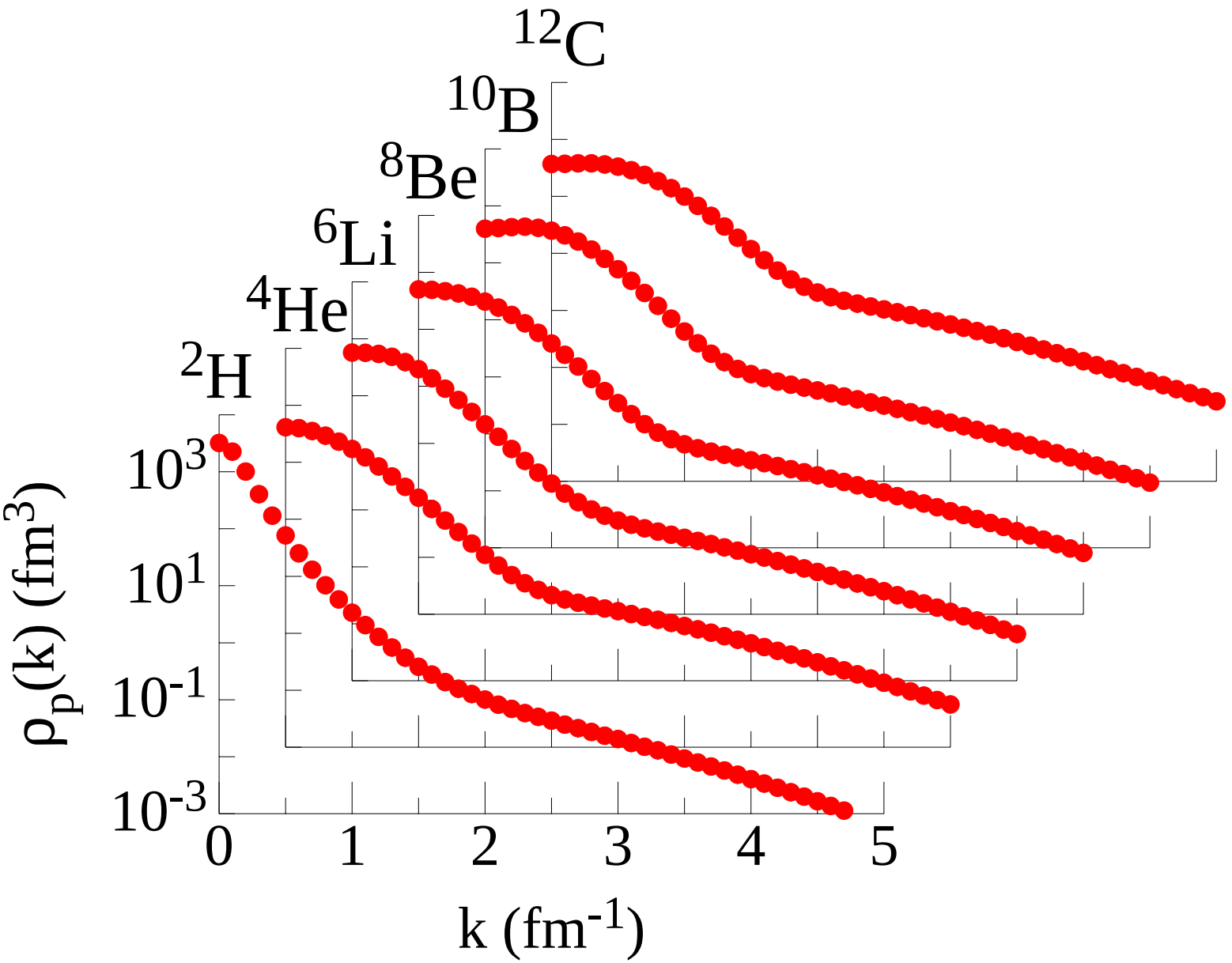

# Two-Nucleon Momentum Distributions

Probability of finding two nucleons in a nucleus with relative momentum $\mathbf{q} = (\mathbf{q}_1 - \mathbf{q}_2)/2$ and total center-of-mass momenta $\mathbf{Q} = (\mathbf{q}_1 + \mathbf{q}_2)$ in a given spin-isospin state:

$$\rho_{NN}(\mathbf{q},\mathbf{Q}) = \int d\mathbf{r}'_1 d\mathbf{r}_1 d\mathbf{r}'_2 d\mathbf{r}_2 d\mathbf{r}_3 \cdots d\mathbf{r}_A \, \psi^{\dagger}_{JM_J}(\mathbf{r}'_1,\mathbf{r}'_2,\mathbf{r}_3,\ldots,\mathbf{r}_A)\, e^{-i\mathbf{q}\cdot(\mathbf{r}_{12}-\mathbf{r}'_{12})}$$

$$e^{-i\mathbf{Q}\cdot(\mathbf{R}_{12}-\mathbf{R}'_{12})}\, P_{NN}(12)\, \psi_{JM_J}(\mathbf{r}_1,\mathbf{r}_2,\mathbf{r}_3,\ldots,\mathbf{r}_A)$$

where $P_{NN}$ is a pair nucleon-nucleon projection operator and the normalization is:

$$N_{NN} = \int \frac{d\mathbf{q}}{(2\pi)^3}\frac{d\mathbf{Q}}{(2\pi)^3}\rho_{NN}(\mathbf{q},\mathbf{Q})$$

and $N_{NN}$ is the total number of given nucleon-nucleon pairs.

This double Fourier transform is evaluated by a double Gauss-Legendre integration over each pair of nucleons in each configuration sampled by the variational Monte Carlo wave function. The angle between $\mathbf{q}$ and $\mathbf{Q}$ can be randomly chosen or at a fixed angle, such as $\mathbf{q}||\mathbf{Q}$.

The proton-proton pair momentum distribution in $^4$He averaged over all angles between $\mathbf{q}$ and $\mathbf{Q}$ is shown as a function of $q$ for fixed values of $Q$. The $pp$ pairs are primarily in relative $^1S_0$ states and show the typical $S$-wave node at $Q = 0$, but this is node is filled in as $Q$ increases.

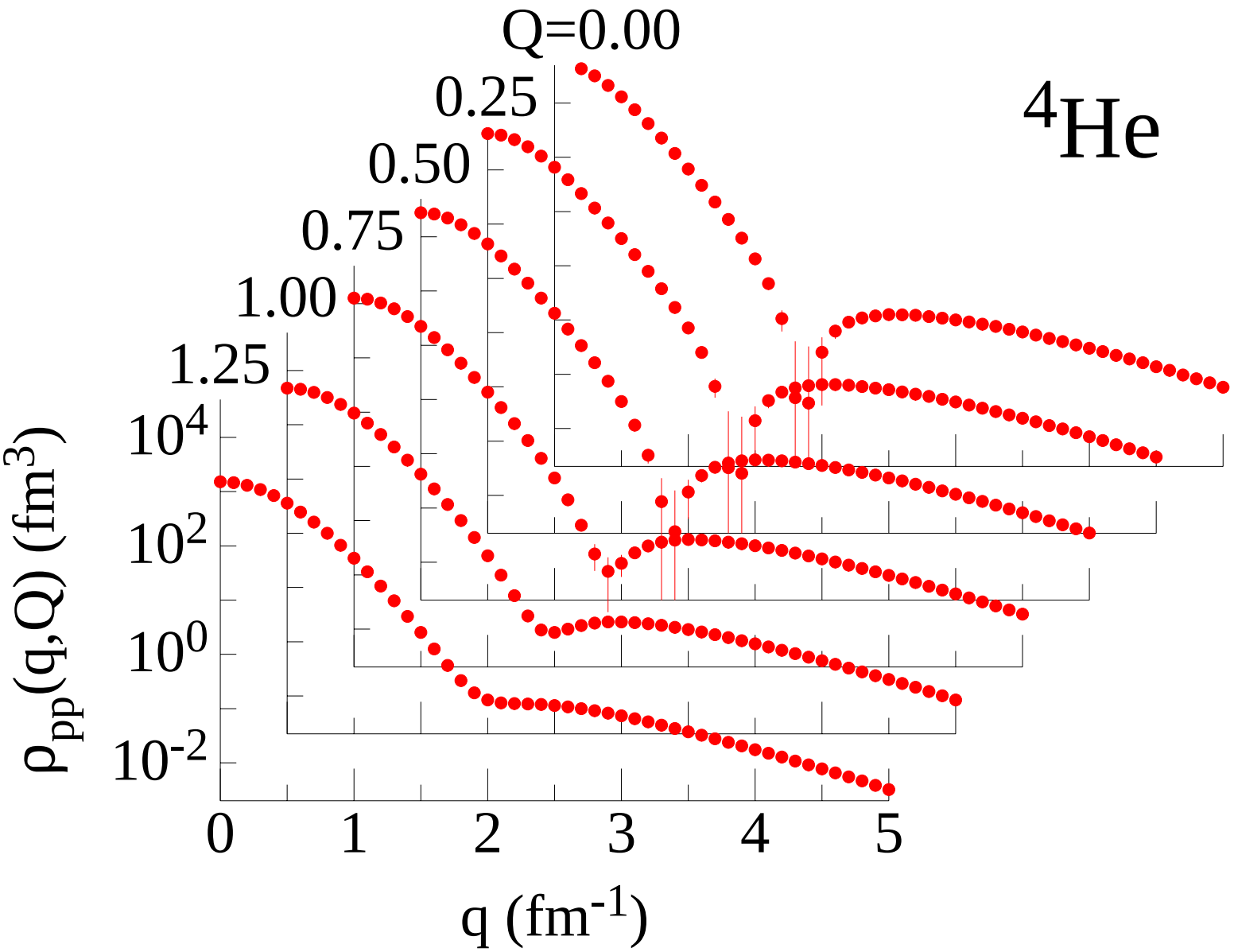

The proton-neutron pairs are mostly in deuteron-like pairs a broad shoulder starting at $q = 2$ fm$^{-1}$ at all $Q$ values. For back-to-back pairs at $Q = 0$, there is a large enhancement in the $pn/pp$ ratio in this region of pair momentum, as observed in recent $(e, e'pN)$ experiments.

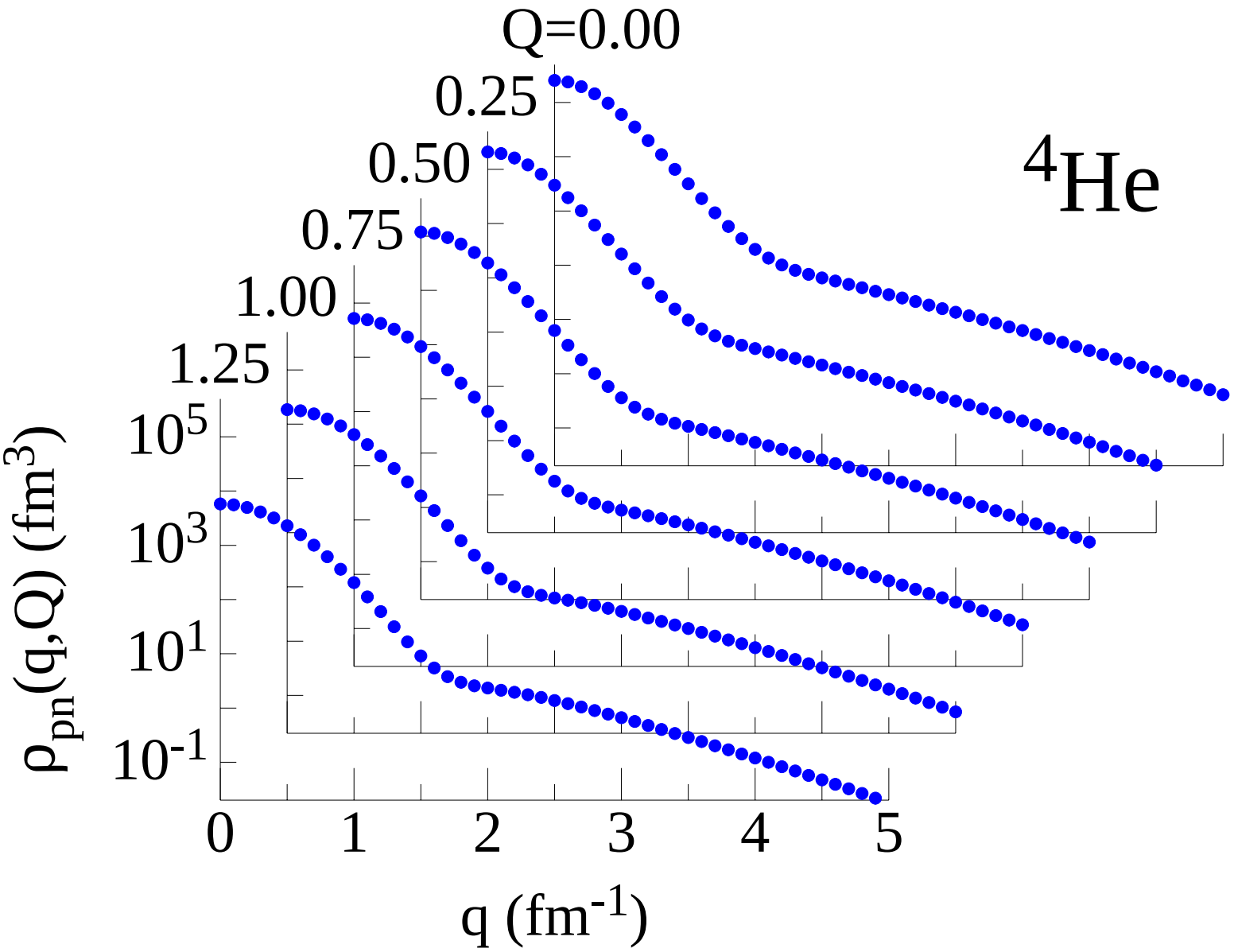

# TABULATIONS

Single-nucleon momentum distributions have been evaluated for many additional $A \leq 12$ cases, as well as cluster-cluster momentum distributions such as $dp$ in $^3$He, $tp$ in $^4$He and $\alpha t$ in $^7$Li. Two-nucleon distributions for $\rho_{NN}(q, Q = 0)$ have also been calculated for many nuclei, as well as cases where $Q$ is integrated over, leaving a $\rho_{NN}(q)$ or alternatively $q$ is integrated over producing a $\rho_{NN}(Q)$.

For anyone who wishes to use these momentum distributions, they are available on-line:

For single-nucleon momentum distributions:

www.phy.anl.gov/theory/research/momenta

For two-nucleon momentum distributions:

www.phy.anl.gov/theory/research/momenta2

Wiringa, Schiavilla, Pieper, & Carlson, PRC **89**, 024305 (2014)

Results used in upcoming experimental PRL on $^4$He$(e, e'pN)$: Korover, et al., arXiv:1401.6138